Journal of Food Engineering 357 (2023) 111650

Contents lists available at ScienceDirect

Journal of Food Engineering

journal homepage: www.elsevier.com/locate/jfoodeng

Microwave heating based on solid-state generators: New insights into heating pattern, uniformity, and energy absorption in foods

Xu Zhou [a], Zhongwei Tang [a], Patrick D. Pedrow [b], Shyam S. Sablani [a], Juming Tang [a,*]

[a] Department of Biological Systems Engineering, Washington State University, Pullman, WA, 99164, USA
[b] School of Electrical Engineering and Computer Science, Washington State University, Pullman, WA, 99164, USA

ARTICLE INFO

Keywords:
Solid-state
Microwave heating
Frequency
Predictable pattern
Energy coupling
Uniformity

ABSTRACT

Microwave (MW) ovens, powered by traditional magnetrons, often produce unpredictable heating patterns in foods due to their wide and random frequency spectrum. This study investigated the potential of solid-state (SS) MW generators to overcome this limitation. The frequency spectra of the SS generator were measured, computer simulation and experimental methods were used to analyze the standing wave and heating patterns within foods. The influence of SS operating frequency on MW power reflection and heating uniformity was also examined. The results show that the SS generator's operating frequency bandwidth was less than 0.1 MHz, approximately 1/500th that of magnetrons. This narrow and stable bandwidth enabled the SS-powered cavity to support a single standing wave pattern (mode), resulting in stable and predictable heating patterns in foods. Moreover, adjusting SS operating frequency could minimize MW power reflection, using complementary SS frequencies could improve MW heating uniformity. This study provides fundamental insights into SS MW heating and offers guidance on controlling SS frequency to improve heating performance.

1. Introduction

Microwave (MW) heating is an efficient method for delivering energy to foods. It has been increasingly utilized in various food processing applications, such as blanching, drying, frying, baking, pasteurization, and sterilization (Tang, 2015; Zhou and Wang, 2019). Since the first invention of the MW oven in 1947, magnetrons have been the primary power source for both domestic and industrial MW heating units (Atuonwu and Tassou, 2018). However, magnetrons have certain limitations that hinder broader applications in the food industry.

One major limitation of magnetrons is the lack of ability to generat peak frequency within a narrow bandwidth (Werner, 2020; Zhou et al., 2023). For example, a magnetron rated for 2450 MHz in a domestic oven produces MW between 2425 and 2475 MHz (Chan and Reader, 2000). In MW cavities that have dimensions of several wavelengths, such as domestic ovens, multiple standing wave patterns and heating patterns of foods may form over this wide frequency range (Chan and Reader, 2000; Metaxas and Meredith, 1993). Such microwave cavities are commonly referred to as multi-mode cavities. Moreover, magnetrons are prone to random "frequency pulling" (Metaxas and Meredith, 1993), where their peak frequency can change due to factors such as aging, power settings, and food load impedance (Resurreccion et al., 2015; Luan et al., 2017; Zhou et al., 2023). Thus, it is extremely difficult to predict the heating patterns of foods in magnetron-powered multi-mode cavities. In the United States, Food and Drug Administration (FDA) mandates stable heating patterns for the production of shelf-stable foods using MW systems, ensuring that cold spots remain in predictable and consistent locations within food packages (Tang, 2015). However, all magnetron-powered domestic MW ovens and industrial systems at 2450 MHz are multi-mode cavities (Metaxas and Meredith, 1993), limiting the use of MW heating for pathogen control in multi-mode cavities (Tang, 2015).

Solid-state (SS) MW generators have the potential to overcome this limitation. In our recent study (Zhou et al., 2023), we demonstrated that SS MW generators provide stable peak microwave frequency with a very narrow bandwidth that are not influenced by the heated subject. But the impact of the unique spectrum generated by SS generators on the formation of standing waves and heating patterns in foods requires further investigation. Several studies have focused on frequency control of SS generators to enhance heating uniformity and energy absorption in MW heating of food, they have not adequately addressed the predictability of heating patterns in food. For example, Taghian Dinani et al. (2021b) conducted a comparative analysis of SS- and magnetron-powered

* Corresponding author. Biological Systems Engineering Washington State University, Pullman, WA, 99164-6120.
E-mail address: jtang@wsu.edu (J. Tang).

https://doi.org/10.1016/j.jfoodeng.2023.111650
Received 13 October 2022; Received in revised form 3 July 2023; Accepted 6 July 2023
Available online 11 July 2023

Nomenclature

$\mathbf{E}$	Electric field intensity (V/m)
$\mathbf{E}_s$	Phasor form of electric field intensity (V/m)
E_{xs}, E_{ys}, E_{zs}	Components of *E*-field (V/m) in the *x*-, *y*-, *z*-directions
E_{rms}	Root mean square of the electric field strength (V/m)
$\mathbf{H}$	Magnetic field intensity (A/m)
$\mathbf{H}_s$	Phasor form of magnetic field intensity (A/m)
H_{xs}, H_{ys}, H_{zs}	Components of *H*-field (V/m) in the *x*-, *y*-, *z*-directions
ω	Angular frequency (rad/s)
ε	Permittivity of free space (=8.854 × 10^{-12} F/m)
μ	Permeability of free space (=4π × 10^{-7} H/m)
$\vec{n}$	Unit vector normal to the boundary
β	Phase constant (rad/m)
$\beta_x, \beta_y, \beta_z$	Components of phase constant β (rad/m) in the *x*-, *y*-, *z*-directions
a, *b*, *c*	Rectangular cavity dimensions in the *x*-, *y*-, *z*-directions
m, *n*, *p*	The number of half-wavelengths of sinusoidal variation of *E*-field in the *x*-, *y*-, and *z*-directions
f_r	Resonant frequency (Hz)

household MW ovens, revealing that energy efficiency and heating uniformity varied depending on the shape and orientation of the tested samples. In another study (Taghian Dinani et al., 2021a), an orderly frequency sweep of the SS generator was shown to yield improved temperature distributions in a model food sample compared to a fixed frequency. Additionally, Yang and Chen (2022) and Yang et al. (2022a & 2022b) proposed dynamic frequency-shifting strategies using closed-loop feedback and an online thermal camera to enhance heating uniformity in an SS-powered MW oven.

The stability and predictability of heating patterns in foods during MW heating are critical in ensuring effective pathogen control (Tang, 2015). Therefore, this study aimed to address two questions:

1) Can SS MW generators provide stable and predictable heating patterns of foods in a multi-mode MW cavity?
2) Can SS MW generators improve heating uniformity and energy efficiency while maintaining stable heating patterns in foods?

Accordingly, this study was conducted with two specific objectives:

1) To develop a mathematical model of standing wave patterns (modes) and experimentally determine the heating patterns of food in a SS-powered MW cavity.
2) To investigate the influence of SS MW frequency on energy coupling and heating uniformity in a SS-powered MW cavity.

2. Materials and methods

2.1. SS MW heating unit

A GaN-based SS MW heating unit was used in this study. The testing unit consisted of three main components: (1) a GaN-based SS generator (RIU58800-20, RFHIC Co., Anyang, South Korea) with a power output of 400 W (Zhou et al., 2022), (2) a MW cavity (410 mm × 320 mm × 250 mm), and (3) a standard waveguide (WR-159) (250 mm × 40 mm × 20 mm) connecting the SS MW generator to the cavity. Fig. 1 shows the schematic diagram and dimensions of the MW heating unit. The SS MW generator had an operating frequency range of 5800 ± 75 MHz, allocated by the Federal Communications Commission (FCC) for ISM applications (Tang, 2015).

2.2. Analytical method to calculate fundamental modes

An electromagnetic field pattern created by standing waves is referred to as a *mode* (Sadiku, 2018). To investigate the sensitivity of the mode to the SS MW frequency, fundamental modes in the empty MW cavity were determined using an analytical approach, as suggested by Chan and Reader (2000). The MW cavity, as shown in Fig. 1A, was modeled as a closed rectangular box with dimensions of 410 mm × 320 mm × 250 mm (Fig. 2A).

Maxwell's equations in phasor form were applied to the empty box (Sadiku, 2018):

$$\nabla^2\mathbf{E}_s + \beta^2\mathbf{E}_s = 0 \tag{1}$$

$$\nabla^2\mathbf{H}_s + \beta^2\mathbf{H}_s = 0 \tag{2}$$

$$\beta = \omega\sqrt{\mu\varepsilon} \tag{3}$$

In the rectangular coordinate system,

$$\mathbf{E}_s = \left(E_{xs}, E_{ys}, E_{zs}\right) \text{ and } \mathbf{H}_s = \left(H_{xs}, H_{ys}, H_{zs}\right) \tag{4}$$

Substituting Eq. (4) into Eqs. (1) and (2), we would obtain six partial differential equations. Taking the *x*-component of $\mathbf{E}_s$ as an example (that is, E_{xs}), Eq. (1) became:

$$\frac{\partial^2 E_{xs}}{\partial x^2} + \frac{\partial^2 E_{xs}}{\partial y^2} + \frac{\partial^2 E_{xs}}{\partial z^2} + \beta^2 E_{zs} = 0 \tag{5}$$

To solve the above wave equations, boundary conditions were applied by assuming the cavity walls to be perfect electric conductors (PECs):

$$\vec{n} \times \mathbf{E} = 0 \tag{6}$$

Using the separation of variables, each component of $\mathbf{E}_s$ and $\mathbf{H}_s$ can be solved. The detailed mathematical solutions of the partial differential equations are in Balanis (2012) and Sadiku (2018). Here, only final formulas were given. There were two modes, transverse electric (TE) and transverse magnetic (TM) modes:

1) TE mode: $E_z = 0$, E_x and E_y are transverse (normal) to wave propagation direction

$$E_x = \left(\frac{j\omega\mu}{h^2}\right)\beta_y H_0 \cos(\beta_x x)\sin\left(\beta_y y\right)\sin\left(\beta_z z\right) \tag{7a}$$

$$E_y = -\left(\frac{j\omega\mu}{h^2}\right)\beta_x H_0 \sin(\beta_x x)\cos\left(\beta_y y\right)\sin\left(\beta_z z\right) \tag{7b}$$

$$E_z = 0 \tag{7c}$$

$$H_x = -\left(\frac{1}{h^2}\right)\beta_x\beta_z H_0 \sin(\beta_x x)\cos\left(\beta_y y\right)\cos\left(\beta_z z\right) \tag{7d}$$

$$H_y = -\left(\frac{1}{h^2}\right)\beta_y\beta_z H_0 \cos(\beta_x x)\sin\left(\beta_y y\right)\cos\left(\beta_z z\right) \tag{7e}$$

$$H_z = H_0 \cos(\beta_x x)\sin\left(\beta_y y\right)\sin\left(\beta_z z\right) \tag{7f}$$

2) TM mode: $H_z = 0$, H_x and H_y are transverse (normal) to wave propagation direction

$$E_x = -\left(\frac{1}{h^2}\right)\beta_x\beta_z E_0 \cos(\beta_x x)\sin\left(\beta_y y\right)\sin\left(\beta_z z\right) \tag{8a}$$

$$E_y = -\left(\frac{1}{h^2}\right)\beta_x\beta_z E_0 \sin(\beta_x x)\cos\left(\beta_y y\right)\sin\left(\beta_z z\right) \tag{8b}$$

$$E_z = E_0 \sin(\beta_x x)\sin\left(\beta_y y\right)\cos\left(\beta_z z\right) \tag{8c}$$

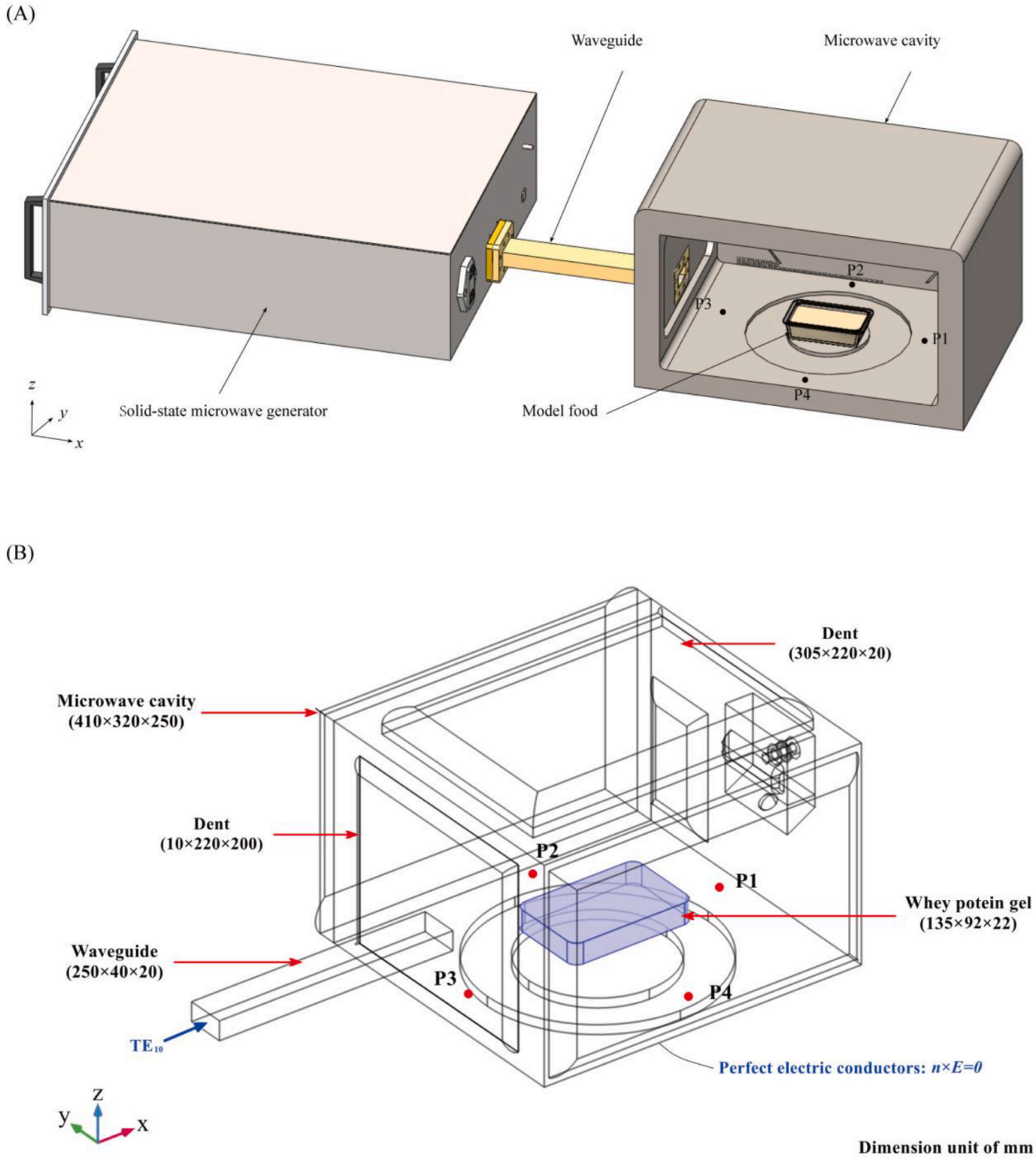

Fig. 1. Solid-state powered microwave oven: **(A)** CAD drawing of the oven with a 5.8 GHz solid-state generator, WR-159 waveguide, microwave cavity, and a model food (whey protein gel), four load positions in the cavity are labeled as P1, P2, P3, and P4; **(B)** corresponding computer simulation model (adapted from Zhou et al., 2023).

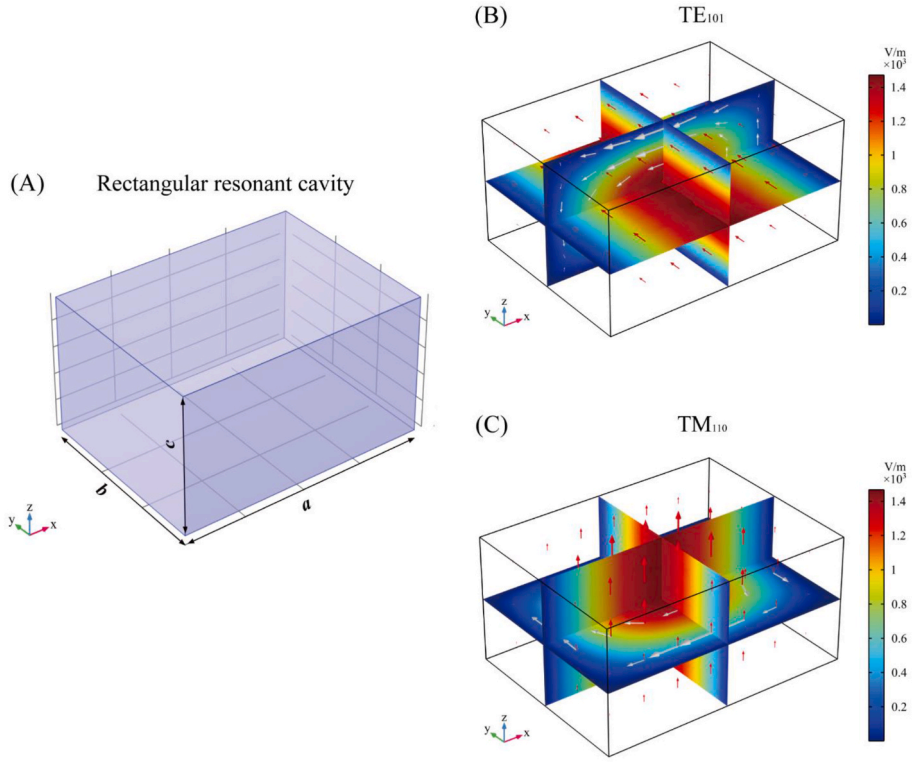

Fig. 2. Resonant cavity and two dominant modes: **(A)** schematic of the resonant cavity with dimensions of $a = 410$ mm, $b = 320$ mm, $c = 250$ mm; microwave field distributions of **(B)** TE_{101} and **(C)** TM_{110} modes (Red arrows stand for electric fields; white arrows stand for magnetic fields).

$$H_x = -\left(\frac{j\omega\varepsilon}{h^2}\right)\beta_y E_0 \sin(\beta_x x)\cos(\beta_y y)\cos(\beta_z z) \tag{8d}$$

$$H_y = -\left(\frac{j\omega\varepsilon}{h^2}\right)\beta_x E_0 \cos(\beta_x x)\sin(\beta_y y)\cos(\beta_z z) \tag{8e}$$

$$H_z = 0 \tag{8f}$$

Eqs. (7) and (8) are associated with

$$\beta_x = \frac{m\pi}{a} \tag{9a}$$

$$\beta_y = \frac{n\pi}{b} \tag{9b}$$

$$\beta_z = \frac{p\pi}{c} \tag{9c}$$

$$h^2 = \beta_x^2 + \beta_y^2 \tag{9d}$$

$$\beta_x^2 + \beta_y^2 + \beta_z^2 = \beta^2 = \omega^2\mu\varepsilon \tag{9e}$$

Certain modes cannot exist; otherwise, all field components will be zero (Balanis, 2012). For TE_{mnp} modes, p cannot be zero, and m and n cannot be zero at the same time (i.e., TE_{mn0} and TE_{00p} do not exist); For TM_{mnp} modes, neither m nor n can be zero (i.e., TM_{0np} and TM_{m0p} do not exist).

Since $\omega = 2\pi f$, from Eqs. (9a), (9b), (9c) and (9e) we obtain the resonant frequency:

$$f_r = \frac{1}{2\pi\sqrt{\mu\varepsilon}}\sqrt{\left(\frac{m\pi}{a}\right)^2 + \left(\frac{n\pi}{b}\right)^2 + \left(\frac{p\pi}{c}\right)^2} \tag{10}$$

where f_r is the resonant frequency (Hz). The resonant frequencies were calculated by MATLAB (R2021a, MathWorks Ltd, Natick, MA, USA). The mode in the resonant cavity with the lowest frequency is the dominant mode (Sadiku, 2018). The dominant mode depends on the cavity dimension. If $a > b < c$, TE_{101} is the dominant mode; If $a < c > b$, TM_{110} is the dominant mode, as illustrated in Fig. 2.

2.3. Computer simulation to visualize modes and heating patterns of foods

A 3-D computer simulation model based on finite-element method (FEM) was previously developed and validated in another study (Zhou et al., 2023). In this study, the developed simulation model was utilized to visualize the impact of the SS MW frequency spectrum on the standing wave modes and heating patterns of foods being heated in the MW cavity. The governing equations, boundary conditions, meshing, and experimental validations of the computer model are described in detail in Zhou et al. (2023).

2.4. Measurement of frequency spectrum

The peak MW frequencies and occupied frequency bandwidth (OFBW), which covers 80% of the total MW power, were determined using a spectrum analyzer (SPA-6G, LATNEX, Toronto, Canada) and a dipole antenna (Data Alliance Inc, Nogales, AZ, USA). The measurement method described by Resurreccion et al. (2015) and Zhou et al. (2023) was used with minor improvements in this study. Specifically, the dipole antenna was positioned 5 cm from the front door of the cavity, and the spectrum analyzer was set to measure MW power amplitudes at 55 discrete frequency points within a 1 MHz frequency span. The frequency interval between any two adjacent measurement points was 18 kHz [1MHz/(55−1) = 0.018 MHz = 18 kHz]. The MW spectrum curve was analyzed by averaging 300 snapshots, according to the method developed by Zhou et al. (2023).

2.5. Determination of power coupling

Power reflection from the MW cavity to the SS generator was used as

an indicator of coupling between the generator and cavity. It was calculated by:

$$PR = \frac{P_r}{P_f} \times 100\% \quad (11)$$

where PR is the reflection (%), P_r is reflected power (W) and P_f is forward power (W).

In microwave heating tests, the P_r and P_f were simultaneously measured by the microwave power detectors built into the SS generator. According to the generator manufacturer (RFHIC Corp.), the power detectors had ± 3% measurement accuracy. The P_f of the generator was set to 400 W, and the P_r was measured at 11 discrete frequencies between 5750 and 5850 MHz, that is, 5750, 5760, 5770 …, 5840, and 5850 MHz, for different food load conditions.

To investigate the effect of food loads on the coupling between the SS generator and the loaded cavity, three food loads with the same mass were used: 300 g of distilled water, 300 g of soybean oil, and 300 g of whey protein gel (WPG). The distilled water was obtained from a Milli-Q purification system (Millipore Co., Billerica, MA, USA), and the soybean oil (Great value brand, Walmart Inc., Bentonville, AR, USA) was purchased from a local grocery store (Pullman, WA, USA). The WPG was prepared using the method described by Resurreccion et al. (2015), which consisted of 75.4% distilled water, 0.3% salt, 0.2% D-ribose, 18.9% whey protein concentrate, and 5.2% whey protein isolate. The water and oil loads were placed in 300-ml cylindrical beakers, and the WPG was placed in a 10.5-oz plastic tray (135 mm × 92 mm × 22 mm). Additionally, distilled water samples of different volumes (300 ml, 1000 ml, and 3000 ml) in glass beakers were used to investigate the influence of sample volume/mass on energy coupling in the SS-powered cavity. Each food sample was positioned centrally on the bottom of the cavity during testing, the turntable was removed since the study was focused on stationary food loads. Furthermore, the 300 ml of distilled water load was positioned at four different locations (P1, P2, P3, and P4) on the cavity bottom, as shown in Fig. 1, to examine the effect of load position on coupling.

2.6. Determination of heating pattern of foods

The model food, WPG (135 mm × 92 mm × 22 mm), was sliced horizontally into two equal-thickness pieces and placed together in a 10.5-oz plastic tray before MW heating (Zhou et al., 2023). The tray was placed centrally at the bottom of the cavity and heated using an SS MW heating unit (5800 MHz) for 60 s. After the heating process, the thermal patterns of the three layers of WPG were immediately captured using a FLIR infrared thermal camera (SC-3000, FLIR Systems, Portland, OR., USA) (Zhou et al., 2023). The cold spot (lowest temperature) and hot spot (highest temperature) in three layers of the whey protein gel were identified by using the thermography Software FLIR Tools 2022 (Teledyne FLIR LLC, Wilsonville, OR., USA). The heating tests were conducted in triplicate runs ($n = 3$).

2.7. Frequency control strategy to improve heating uniformity

Based on the results of Section 2.5, we initially selected several frequencies where the measured power reflections of the model food were below 10%, indicating more than 90% net power absorption. These frequencies included 5750, 5760, 5770, 5820, and 5840 MHz. Next, we determined the heating patterns of WPG at these frequencies. After analyzing the thermal image data, we finalized two frequencies (5770 and 5840 MHz) to create a complimentary heating pattern (which will be discussed later). The frequency control strategy involved: 1) heating the WPG at 5770 MHz for 30 s, and then 2) heating at 5840 MHz for another 30 s. The resulting heating patterns were compared to those obtained at each of the two fixed frequencies (5770 and 5840 MHz). To evaluate the heating uniformity, temperature differences between the cold and hot spots were calculated. Additionally, uniformity index (UI) in food samples was determined to quantify the spatial temperature distribution (Alfaifi et al., 2014). The UI was calculated from:

$$UI = \frac{\int_{V_{vol}} |T - T_{av}| dV_{vol}}{(T_{av} - T_{\text{initial}}) V_{vol}} \quad (12)$$

where T, T_{av}, and T_{initial} are the local, average, and initial temperatures (°C) of a food sample, respectively, and V_{vol} is the volume of the sample (m^3).

3. Results and discussion

3.1. Single standing wave patterns (modes) in SS MW cavities

Resonant frequencies and their associated modes in an empty MW cavity were calculated using both analytical method and computer simulation over a frequency range of 5750–5850 MHz (Table 1). The simulation results matched well with the analytical results, with a maximum difference of less than 0.1% (Table 1), validating the accuracy of the computer simulation model. Based on Eqs. (7) and (8), modes with different integers m, n, and p have different E-field patterns. Table 1 shows that the rectangular MW cavity supported more than 40 different modes over the above frequency range (i.e., 100MHz). It's worth noting that modes were highly sensitive to frequency variations in the multimode cavity; slight changes in frequency resulted in significant differences in the standing wave patterns (Fig. 3). For example, TE_{908} at 5817 MHz and TM_{985} at 5819 MHz had a totally different standing wave pattern, as shown in Fig. 3.

When the MW cavity was loaded with a food tray (135 mm × 92 mm × 22 mm), the regular modes were distorted. However, the E-fields still showed similar sensitivity in response to MW frequency. Fig. 4 illustrates the influence of 10 MHz increments in the MW frequency on the distribution of the E-field within the loaded cavity. In consumer MW ovens, magnetrons typically operate within a frequency spectrum of 20–70 MHz (Chan and Reader, 2000; Metaxas and Meredith, 1993; Werner, 2020; Zhou et al., 2023). As an example, let's consider a specific frequency range of 5780–5830 MHz, representing a bandwidth of 50 MHz. Within this frequency range, the loaded MW cavity can support multiple different E-fields (Fig. 4). Temperature distribution within a

Table 1
Standing wave patterns (modes) in an empty microwave cavity (410 mm × 320 mm × 250 mm) over a frequency range between 5750 and 5850 MHz.

Mode type	m	n	p	Calculated frequency (MHz)[a]	Simulated frequency (MHz)[b]	Error (%)
TE, TM[c]	2	4	9	5759.1	5759.5	0.007
TE, TM	6	7	7	5760.3	5760.7	0.007
TE, TM	4	3	9	5765.0	5765.4	0.007
TE, TM	6	5	8	5771.2	5771.7	0.009
TE, TM	7	9	5	5771.7	5772.1	0.007
TE, TM	5	2	9	5774.1	5774.6	0.009
TE, TM	7	8	6	5791.1	5791.5	0.007
TE, TM	8	3	8	5791.3	5791.7	0.007
TE	0	7	8	5810.5	5810.9	0.007
TE, TM	4	8	7	5813.7	5814.1	0.007
TE, TM	3	4	9	5816.8	5817.3	0.009
TE	9	0	8	5816.9	5817.4	0.009
TE, TM	9	8	5	5818.9	5819.3	0.007
TE, TM	1	7	8	5822.0	5822.4	0.007
TE, TM	9	5	7	5824.9	5825.1	0.003
TE	6	0	9	5825.2	5825.7	0.008
TE, TM	9	1	8	5835.8	5836.2	0.007
TE, TM	5	9	6	5836.0	5837.5	0.026
TE, TM	8	6	7	5837.0	5839.7	0.046
TE, TM	6	1	9	5844.0	5844.5	0.009

[a] From Eq. (10) (analytical method).
[b] From computer simulation (numerical method).
[c] TE mode: transverse electric mode; TM mode: transverse magnetic mode.

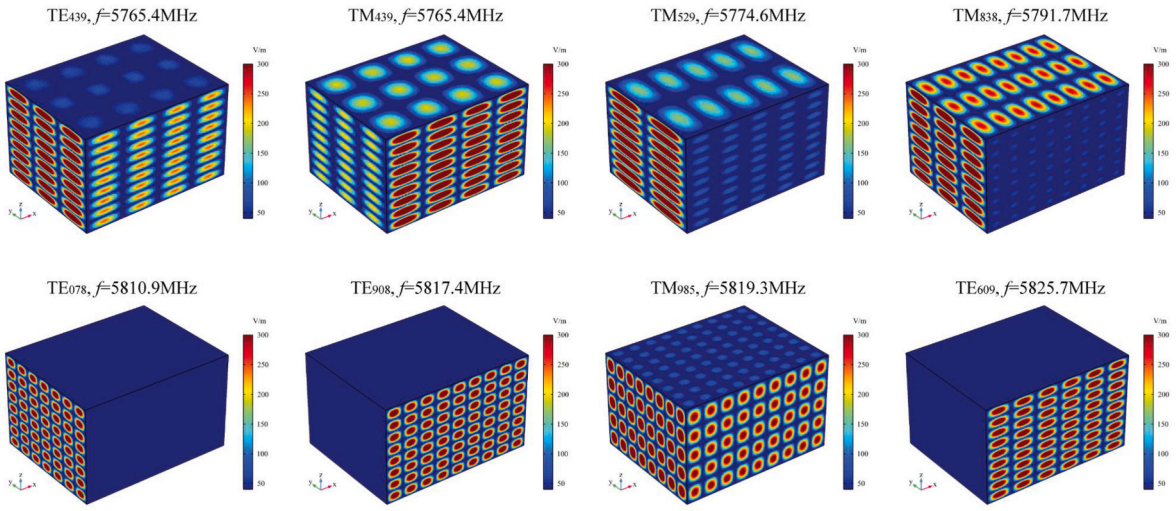

Fig. 3. Simulated standing wave patterns (V/m) at various frequencies in an empty microwave cavity (Fig. 2A).

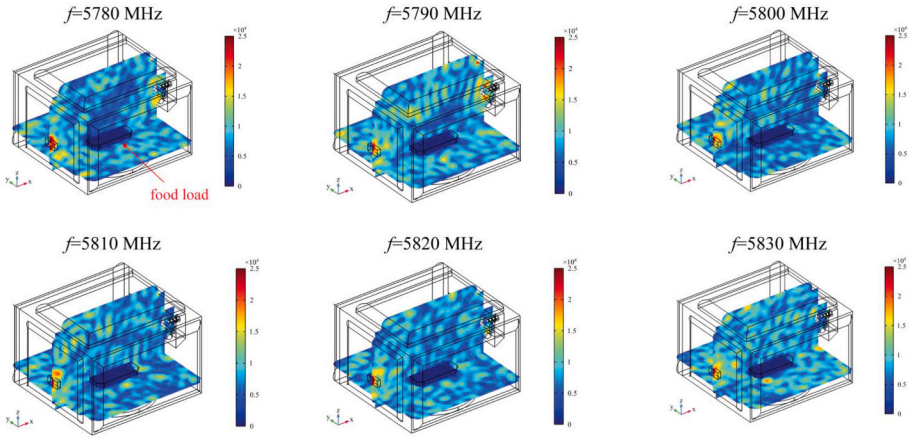

Fig. 4. Simulated electric field patterns (V/m) at six selected frequencies when the food load (whey protein gel) (135 mm × 92 mm × 22 mm) was introduced into the microwave cavity (Fig. 1B).

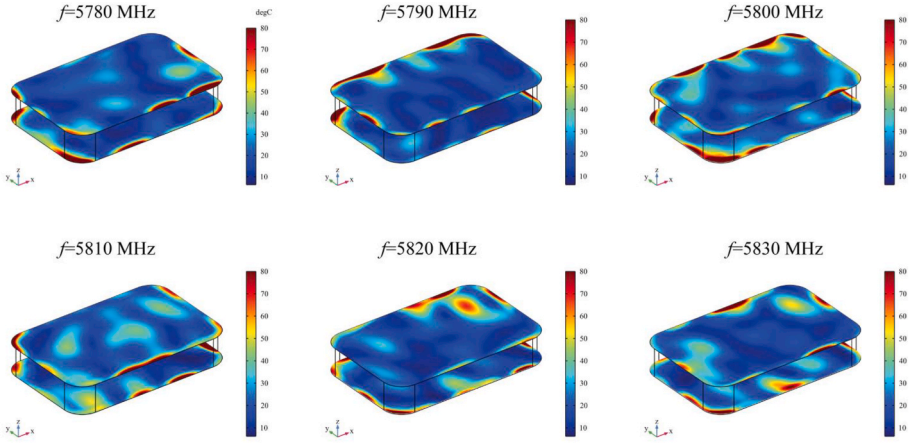

Fig. 5. Simulated temperature distribution (°C) of the top and bottom layers of the food load (whey protein gel) (135 mm × 92 mm × 22 mm) at six selected frequencies.

food load directly corresponds to the distribution of *E*-fields. Fig. 5 shows the temperature distribution in the food tray as influenced by the peak MW frequency. Even a small 10 MHz increment resulted in changes in the locations of cold and hot spots within the model food. This highlights the challenge of accurately predicting heating patterns in a magnetron-powered multi-mode cavity, due to the wide bandwidth (e.g., 20–70 MHz) (Chan and Reader, 2000; Werner, 2020) and random operating frequency associated with magnetron generators (Luan et al.,

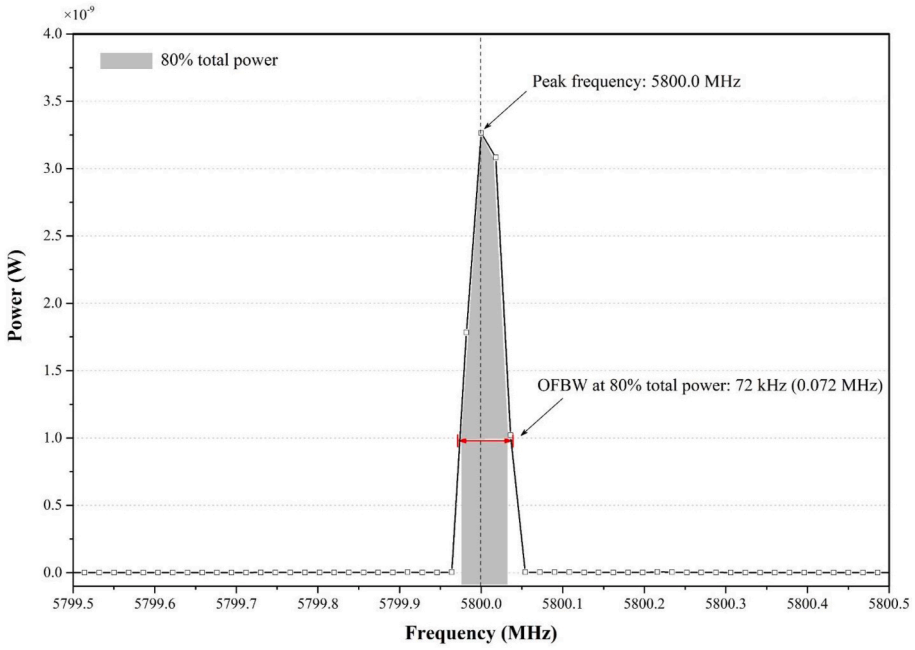

Fig. 6. Measured frequency spectrum of a solid-state generator, including peak frequency and occupied frequency bandwidth (OFBW, covering 80% total power). The generator was set to 5800 MHz. $n = 3$.

2017; Zhou et al., 2023).

In comparison to magnetron generators, the SS generator produced microwaves within a much narrower frequency bandwidth (Fig. 6). The occupied frequency bandwidth of the SS generator, which accounted for 80% of the total power, measured only 0.072 MHz (Fig. 6). This bandwidth is approximately 1/500th of the frequency bandwidth typically observed in magnetron generators (20–70 MHz) (Chan and Reader, 2000; Zhou et al., 2023). More testing conducted with other set frequencies, such as 5750, 5760, 5770 …, 5800, 5810 …, and 5850 MHz, consistently demonstrated that the SS generator produced microwaves within a narrow frequency bandwidth of less than 0.1 MHz for each set frequency (data not shown). Considering that adjacent resonant frequencies in the cavity differed by at least 0.2 MHz (as indicated in Table 1), the narrow frequency bandwidth of the SS generator (less than 0.1 MHz for any set frequency) ensured that only a single standing wave pattern can form within the cavity. As a result, the SS generator offers better predictability and control over the standing wave and, consequently, the heating pattern of foods compared to magnetron

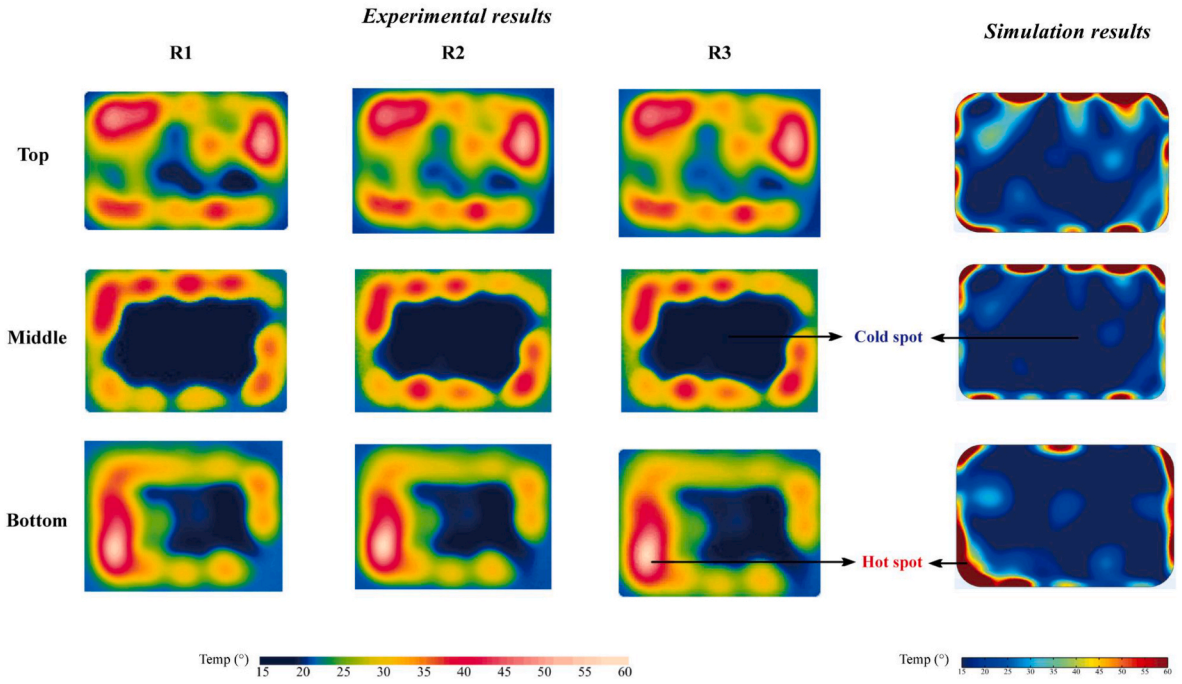

Fig. 7. Comparison of heating patterns between experimental results (n = 3) and simulation results (adapted from Zhou et al., 2023). The heating pattern shows the temperature distribution of the top, middle, and bottom layers of whey protein gel after being heated in a 400 W solid-state microwave cavity (5800 MHz) for 60 s. The arrows indicate the locations of cold and hot spots.

generators.

3.2. Stable and predictable heating pattern of foods in SS MW cavities

The experimental heating pattern for the WPG in the SS-powered cavity confirmed that a single standing wave mode generated by the SS generator would result in a stable and predictable heating pattern of foods (Fig. 7). The heating patterns of WPG were consistent between three replications, demonstrating the stability and repeatability of the SS-powered MW cavity. In contrast, previous studies have revealed that magnetron-powered domestic MW cavities tend to produce inconsistent heating patterns and large temperature deviations of food samples between replications (Pitchai et al., 2012, 2014, 2015). The computer simulation accurately predicted the locations of cold and hot spots in the SS-powered MW oven and showed good agreement with experimental results, as shown in Fig. 7. There were some discrepancies between the experimental and simulated results, primarily due to the simplified geometries of the food sample and the oven cavity used in the simulation. To improve the accuracy of predictions, future simulations could incorporate advanced techniques, such as 3-D scanning, to capture the precise shape of the MW oven and food samples, as suggested by Yi et al. (2021) and Zhang et al. (2020). Overall, our study demonstrates that SS MW generators could produce stable and predictable heating patterns of foods in a multi-mode MW cavity.

3.3. Heating performance

3.3.1. Power coupling

Efficient coupling is an important consideration in the design of MW systems and the development of MW-assisted food processing. In this study, power reflection, which is an indicator of MW coupling efficiency, was measured as a function of SS frequency for different food loads, positions, and volumes. Our results revealed significant variations in microwave power reflection, as influenced by load type and volume, over the frequency range between 5750 and 5850 MHz that can be provided by the GaN-based SS generator (RIU58800-20) used in this study (Figs. 8–10). For example, water had the least power reflection at 5810 MHz, whereas WPG had the highest reflection at 5810 MHz (Fig. 8). Also, the power reflection at 5810 MHz increased from 0% to 20% when the water load was moved from location P2 to P3, mimicking a ¼ turntable rotation (Fig. 10). In magnetron-based MW ovens, it is generally observed that the power reflection decreases as the food volume increases (Buffler, 1993). However, in the case of the SS-powered MW oven, the power reflection did not always decrease with increasing food volume at a given frequency (Fig. 9). For example, at 5840 MHz, the 300 ml water load had a smaller power reflection (2%) compared to the 1000 ml (13%) and 3000 ml (9%) water loads. In traditional magnetron-powered MW ovens, the operating frequency bandwidth of the magnetron is typically broad and can accommodate various food loads (Metaxas and Meredith, 1993; Zhou et al., 2023). However, in SS-powered MW ovens, the operating frequency of the SS generator is narrow, with a bandwidth of less than 0.1 MHz. Consequently, the SS-powered MW generator cannot cover many resonant frequencies that correspond to various food products. Thus, achieving optimal coupling efficiency in SS-powered MW heating systems is more complex and dependent on specific characteristics of the food load and MW cavity.

To address these challenges and ensure desirable net MW power, our recommended approach is to sweep the SS frequency and measure power reflection within the loaded MW cavity prior to food processing. Based on the obtained power reflection data, suitable SS frequencies can be selected to achieve the desired net MW power and optimize coupling efficiency.

3.3.2. Heating uniformity

The SS frequency selection is also important for MW heating uniformity. The thermal images of the WPG heated for 60 s at two separate frequencies (5770 or 5840 MHz) showed severe non-uniform heating

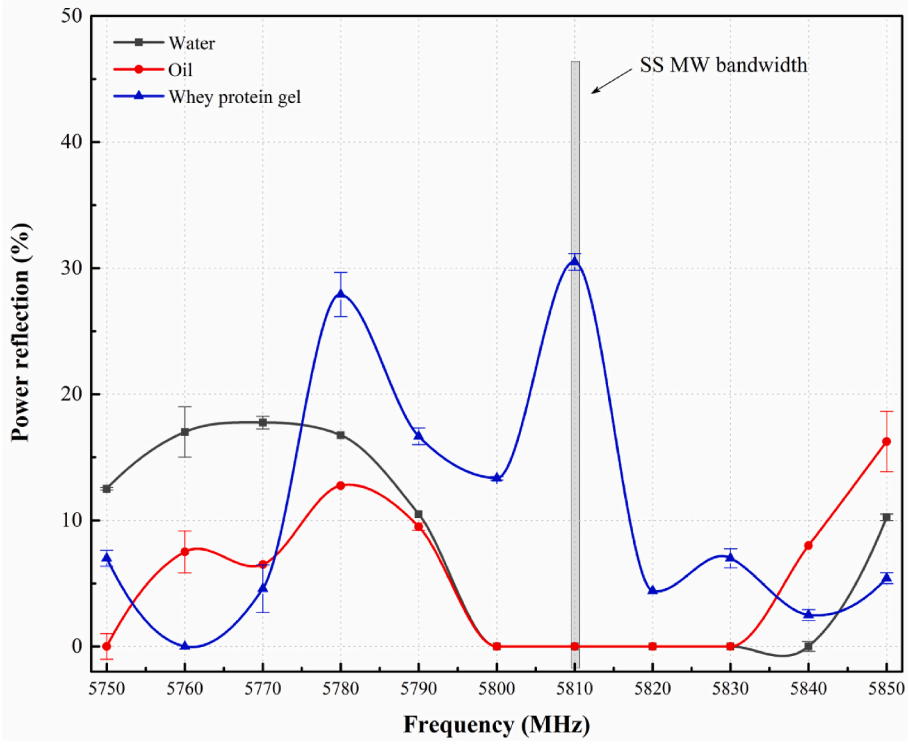

Fig. 8. Measured microwave power reflections (Ave ± SD, $n = 3$) at different frequencies for three different food loads (water, oil, and whey protein gel) with the same mass (300 g) placed centrally at the bottom of the cavity. The grey area indicates the occupied frequency bandwidth (covering 80% total power) of the solid-state generator.

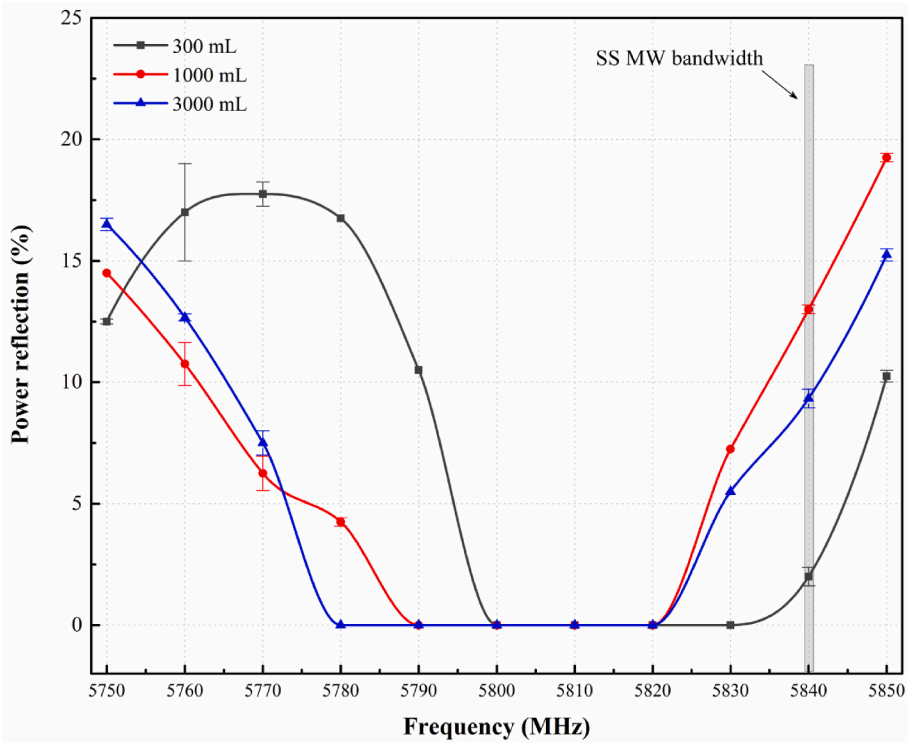

Fig. 9. Measured microwave power reflections (Ave ± SD, n = 3) at different frequencies for water of different volumes (300, 1000, and 3000 mL) placed centrally on the bottom of the cavity. The grey area indicates the occupied frequency bandwidth (covering 80% total power) of the solid-state generator.

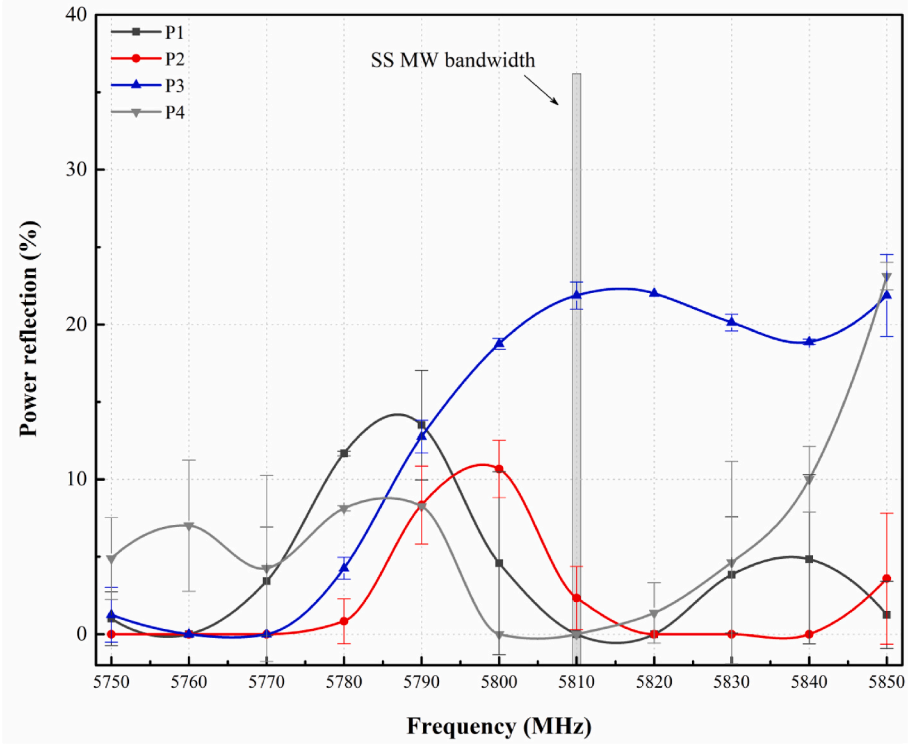

Fig. 10. Measured microwave power reflections (Ave ± SD, $n = 3$) at different frequencies for 300 mL water loads placed at four different positions (P1, P2, P3, and P4 as shown in Fig. 1). The grey area indicates the occupied frequency bandwidth (covering 80% total power) of the solid-state generator.

(Fig. 11). However, when two complementary frequencies were utilized, the non-uniform heating was greatly improved. Specifically, there was a cold zone on the left area of the WPG at 5770 MHz, whereas the same area was relatively hot at 5840 MHz (top layer) (Fig. 11). By combining 5770 MHz and 5840 MHz, the temperature distribution was evened out, resulting in a more uniform temperature distribution compared to using either frequency alone.

To quantitatively assess heating uniformity, temperature differences

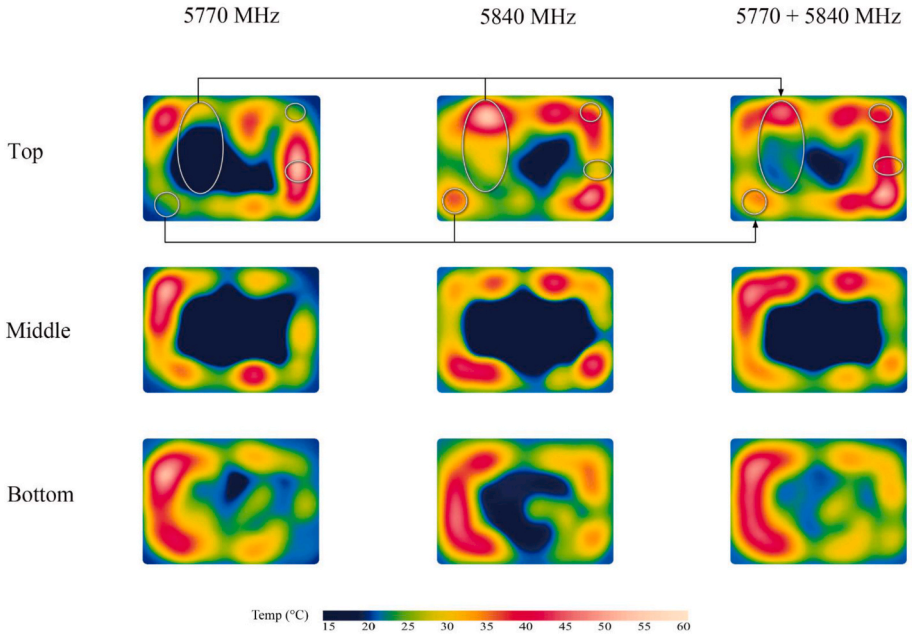

Fig. 11. Experimental heating patterns of top, middle, and bottom layers of whey protein gel. The whey protein gel samples were placed centrally on the cavity bottom and heated from 4 °C at two fixed frequencies (5770 and 5840 MHz for 60 s) and a complementary frequency (5770 MHz for 30 s + 5840 MHz for 30 s) in a 400 W solid-state microwave oven. One thermal image, selected from three replications, is presented to illustrate the results.

Table 2
Temperature differences (°C, Ave ± SD) between cold and hot spots and uniformity index (UI) of whey protein gel heated at different microwave frequencies*.

		5770 MHz	5840 MHz	5770 + 5840 MHz
Temperature difference (°C)	Top layer	45.0 ± 0.8^{a}**	40.8 ± 0.6^{b}	32.5 ± 0.8^{c}
	Middle layer	42.7 ± 2.5^{a}	35.0 ± 0.4^{b}	35.8 ± 1.7^{b}
	Bottom layer	34.9 ± 3.2^{a}	28.5 ± 2.0^{b}	25.1 ± 0.3^{c}
UI	Total volume	0.869	0.732	0.576

* The food samples were heated at three different conditions: (1) heating at 5770MHz for 60 s; (2) heating at 5840MHz for 60s, (3) heating at 5770MHz for 30s followed by heating at 5840MHz for 30s. ** Different lowercase letters indicate that there is a significant difference ($p \leq 0.05$).

between the cold and hot spots within the sample were measured (Table 2). For both the top and bottom layers of the sample, the temperature difference in the sample heated at two complementary frequencies was significantly smaller ($p \leq 0.05$) compared to that heated at two individual frequencies. In addition, the UI (uniformity index) value for the samples heated at two complementary frequencies was lower than that at the single frequency, indicating a more uniform volumetric temperature distribution (Table 2). While we used two frequencies to illustrate this complementary heating pattern concept, it is important to note that more SS frequencies can be selected depending on MW applicators and food loads.

It should be noted that the shallow penetration depth of 5.8 GHz microwaves resulted in cold zones in the middle layer of food samples, regardless of single or combined SS frequencies (Fig. 11). Additionally, edge heating remained a challenge even with the use of complementary frequencies. The edge heating is caused by the reflection and refraction of microwaves at the air-food boundary (Buffler, 1993; Zhou et al., 2023), and it cannot be eliminated solely by controlling SS MW frequency. To address the issue of edge heating, other approaches, such as water immersion, have been used in industrial MW-assisted thermal sterilization and pasteurization systems (Pathak et al., 2003; Tang, 2015). Combining these approaches with the complementary frequency strategy may result in more uniform heating and ensure food safety in industrial MW applications.

3.4. Significance of this work

To ensure microbial safety of processed food, regulatory agencies (such as FDA) require that an industrial MW sterilization or pasteurization system heats food packages with a stable heating pattern (Tang, 2015). This requirement is currently fulfilled by 915 MHz single-mode MW cavities that have well-defined standing wave patterns in heated foods (Pathak et al., 2003; Resurreccion et al., 2015; Tang, 2015). However, single-mode cavities operating at frequencies such as 2450 MHz or 5800 MHz are limited in size and too small for heating single-meal-sized packages (Tang, 2015).

Our study demonstrates that a SS-powered multi-mode oven can provide a single standing wave mode, resulting in a stable and predictable heating pattern that can meet FDA requirements for industrial MW thermal processing. This finding, which has not been previously reported in the literature, provides new insight into the proper design of industrial SS microwave heating systems. By utilizing large multi-mode MW cavities powered by SS generators, food companies can now develop MW thermal processes that can meet the requirements set by regulatory agencies.

4. Conclusions

In conclusion, this study has demonstrated the potential of using a SS-powered multi-mode cavity to provide stable and predictable heating patterns of foods. Unlike magnetron generators that support multiple modes in large cavities, the narrow frequency bandwidth of the SS

generator enabled the formation of a single MW standing wave pattern, resulting in consistent and predictable heating patterns in foods. Furthermore, appropriately adjusting the peak frequencies of the SS generator can effectively reduce MW power reflection. Employing complementary SS MW frequencies can improve MW heating uniformity while maintaining efficient energy absorption in the food samples. These findings emphasize the advantages of SS technology in enabling controlled and efficient MW heating processes in the food industry.

Credit author statement

Xu Zhou: Conceptualization, Methodology, Software, Formal analysis, Investigation, Data curation, Writing - Original draft, Project administration; **Zhongwei Tang**: Conceptualization, Writing - Review & Editing; **Patrick D. Pedrow**: Methodology, Writing - Review & Editing; **Shyam S. Sablani**: Methodology, Writing - Review & Editing; **Juming Tang**: Conceptualization, Resources, Writing - Review & Editing, Supervision, Project administration.

Declaration of competing interest

The authors declare that they have no known competing financial interests or personal relationships that could have appeared to influence the work reported in this paper.

Data availability

Data will be made available on request.

Acknowledgments

We acknowledge the support provided by USDA NIFA (#2020-67017-31194 and #2016-68003-24840) and USDA Hatch project (#101636) for funding this research. Additionally, we express our gratitude to the Mechanical Engineering Workshop at Washington State University for their assistance in fabricating the solid-state microwave heating unit.

References

Alfaifi, B., Tang, J., Jiao, Y., Wang, S., Rasco, B., Jiao, S., Sablani, S., 2014. Radio frequency disinfestation treatments for dried fruit: model development and validation. J. Food Eng. 120, 268–276.

Atuonwu, J.C., Tassou, S.A., 2018. Quality assurance in microwave food processing and the enabling potentials of solid-state power generators: a review. J. Food Eng. 234, 1–15.

Balanis, C.A., 2012. Advanced Engineering Electromagnetics, second ed. John Wiley & Sons, Hoboken, New Jersey.

Buffler, R.C., 1993. Microwave Cooking and Processing. Springer US, New York (Van Nostrand Reinhold).

Chan, T.V.C.T., Reader, H.C., 2000. Understanding Microwave Heating Cavities. Artech House, Boston.

Luan, D.L., Wang, Y.F., Tang, J.M., Jain, D., 2017. Frequency distribution in domestic microwave ovens and its influence on heating pattern. J. Food Sci. 82 (2), 429–436.

Metaxas, A.C., Meredith, R.J., 1993. Industrial Microwave Heating. Peter Peregrinus, London, UK.

Pathak, S.K., Liu, F., Tang, J., 2003. Finite difference time domain (FDTD) characterization of a single mode applicator. J. Microw. Power Electromagn. Energy 38 (1), 37–48.

Pitchai, K., Birla, S.L., Jones, D., Subbiah, J., 2012. Assessment of heating rate and non-uniform heating in domestic microwave ovens. J. Microw. Power Electromagn. Energy 46 (4), 229–240.

Pitchai, K., Chen, J., Birla, S., Gonzalez, R., Jones, D., Subbiah, J., 2014. A microwave heat transfer model for a rotating multi-component meal in a domestic oven: development and validation. J. Food Eng. 128, 60–71.

Pitchai, K., Chen, J., Birla, S., Jones, D., Gonzalez, R., Subbiah, J., 2015. Multiphysics modeling of microwave heating of a frozen heterogeneous meal rotating on a turntable. J. Food Sci. 80 (12), E2803–E2814.

Resurreccion, F.P., Luan, D., Tang, J., Liu, F., Tang, Z., Pedrow, P.D., Cavalieri, R., 2015. Effect of changes in microwave frequency on heating patterns of foods in a microwave assisted thermal sterilization system. J. Food Eng. 150, 99–105.

Sadiku, M.N.O., 2018. Elements of Electromagnetics, seventh ed. Oxford University Press, New York.

Taghian Dinani, S., Feldmann, E., Kulozik, U., 2021a. Effect of heating by solid-state microwave technology at fixed frequencies or by frequency sweep loops on heating profiles in model food samples. Food Bioprod. Process. 127, 328–337.

Taghian Dinani, S., Jenn, A., Kulozik, U., 2021b. Effect of vertical and horizontal sample orientations on microwave heating uniformity produced by magnetron and solid-state generators. Foods 10 (9), 1986. https://doi.org/10.3390/foods10091986.

Tang, J., 2015. Unlocking potentials of microwaves for food safety and quality. J. Food Sci. 80 (8), E1776–E1793.

Werner, K., 2020. The impact of solid-state RF technology on product development. In: Erle, U., Pesheck, P., Lorence, M. (Eds.), Development of Packaging and Products for Use in Microwave Ovens, second ed. Woodhead Publishing, pp. 415–431.

Yang, R., Chen, J., 2022. Dynamic solid-state microwave defrosting strategy with shifting frequency and adaptive power improves thawing performance. Innovat. Food Sci. Emerg. Technol. 81, 103157.

Yang, R., Fathy, A.E., Morgan, M.T., Chen, J., 2022a. Development of a complementary-frequency strategy to improve microwave heating of gellan gel in a solid-state system. J. Food Eng. 314, 110763.

Yang, R., Fathy, A.E., Morgan, M.T., Chen, J., 2022b. Development of online closed-loop frequency shifting strategies to improve heating performance of foods in a solid-state microwave system. Food Res. Int. 154, 110985.

Yi, Z., Qiu, W., Jiao, Y., Row, K.H., Cheng, Y.D., Jin, Y., 2021. Calculation of electric field and temperature distribution within a microwave oven with realistic geometric features geometric features using numeric simulations. J. Microw. Power Electromagn. Energy 55 (1), 3–27.

Zhang, R., Li, F., Tang, J., Koral, T., Jiao, Y., 2020. Improved accuracy of radio frequency (RF) heating simulations using 3D scanning techniques for irregular-shape food. Lebensm. Wiss. Technol. 121, 108951.

Zhou, X., Wang, S.J., 2019. Recent developments in radio frequency drying of food and agricultural products: a review. Dry. Technol. 37 (3), 271–286.

Zhou, X., Zhang, S., Tang, Z., Tang, J., Takhar, P.S., 2022. Microwave frying and post-frying of French fries. Food Res. Int. 159, 111663.

Zhou, X., Pedrow, P.D., Tang, Z., Bohnet, S., Sablani, S.S., Tang, J., 2023. Heating performance of microwave ovens powered by magnetron and solid-state generators. Innovat. Food Sci. Emerg. Technol. 83, 103240.